Molecular dynamics study of the structural basis of dysfunction and the modulation of

reactive oxygen species generation by pathogenic mutants of human dihydrolipoamide

dehydrogenase

Attila Ambrus[a] and Vera Adam-Vizi[a,*]

[a]Department of Medical Biochemistry, Semmelweis University, Budapest, 1094, Hungary

To whom correspondence should be addressed at: Department of Medical Biochemistry,

Semmelweis University, 37-47 Tuzolto St., Budapest, 1094, Hungary, Tel: +361 266 2773,

Fax: +361 267 0031, email: adam.veronika@med.semmelweis-univ.hu

Abstract

Human dihydrolipoamide dehydrogenase (LADH, E3) is a component in the pyruvate-, alpha-ketoglutarate- and branched-chain ketoacid dehydrogenase complexes and in the glycine cleavage system. The pathogenic mutations of LADH cause severe metabolic disturbances, called E3 deficiency that often involve cardiological and neurological symptoms and premature death. Our laboratory has recently shown that some of the known pathogenic mutations augment the reactive oxygen species (ROS) generation capacity of LADH, which may contribute to the clinical presentations. A recent report concluded that elevated oxidative stress generated by the above mutants turns the lipoic acid cofactor on the E2 subunits dysfunctional. In the present contribution we generated by molecular dynamics (MD) simulation the conformation of LADH that is proposed to be compatible with ROS generation. We propose here for the first time the structural changes, which are likely to turn the physiological LADH conformation to its ROS-generating conformation. We also created nine of the pathogenic mutants of the ROS-generating conformation and again used MD simulation to detect structural changes that the mutations induced in this LADH conformation. We propose the structural changes that may lead to the modulation in ROS generation of LADH by the pathogenic mutations.

Keywords: lipoamide dehydrogenase; mutation; reactive oxygen species; diaphorase; molecular dynamics

Abbreviations used:

LADH, (dihydro)lipoamide dehydrogenase; PDHc, pyruvate dehydrogenase complex; α-KGDHc, alpha-ketoglutarate dehydrogenase complex; LA, lipoic acid; ROS, reactive oxygen species; DCPIP, 2,6-dichlorophenolindophenol; RMSD, root mean square deviation; CD, circular dichroism; FAD, flavin adenine dinucleotide; NAD^+/NADH, nicotinamide adenine dinucleotide (oxidized/reduced); MD, molecular dynamics; S.E.M., standard error of the mean; WT, wild-type.

Introduction

Human dihydrolipoamide dehydrogenase (EC 1.8.1.4, LADH, DLD, E3 component, gene: *dld*) is a subunit of pyruvate dehydrogenase (PDHc), alpha-ketoglutarate dehydrogenase (α-KGDHc), branched-chain ketoacid dehydrogenase multienzyme complexes and the glycine cleavage system. In the physiological (forward) direction LADH oxidizes the complex-bound dihydrolipoic acid moiety while generating NADH from NAD^+. When the reverse reaction is modeled *in vitro*, isolated LADH [1, 2] oxidizes NADH while reducing model substrates, like lipoic acid or lipoamide [3]. In both directions in the absence of added electron acceptors, O_2 is reduced by LADH to superoxide ("oxidase reaction" of LADH), the latter being a reactive oxygen species (ROS), which is then partly dismutated to H_2O_2 and O_2 [3-6]. Analogous mechanism to ROS generation by LADH is the diaphorase activity of the enzyme [7], where LADH reduces *via* NADH various ions or organic molecules as artificial substrates [8-10]. The pH optimum of the diaphorase/ROS-generating activity is below 6 (4.8-5.7) [3, 8, 10, 11], while that of the reverse reaction is 6.5-7.3 [8, 10]. pH optimum of the forward physiological reaction is 7.9-8.3 [10, 12].

α-KGDHc generates ROS under pathologically relevant conditions (elevated $NADH/NAD^+$ ratio and acidosis) [3, 13-15] and is considered to be a major source of oxidative stress related to senescence/aging, ischemia–reperfusion and neurodegenerative diseases [14, 16-18]. α-KGDHc is also a sensitive target of ROS in mitochondria [19-23]. ROS generation by α-KGDHc was directly ascribed to the E3-subunit (LADH) [13, 14]. The reason why ROS generation by α-KGDHc is the most significant among the multienzyme complexes bearing LADH is still obscure [24]. There are strong indications that LADH may also exist as an individual enzyme, and potentially generates ROS, independent of multienzyme complexes [3, 25, 26]. The only crystal structure that represents the non-complexed form of human LADH is by Brautigam et al. [27].

The LADH flavoprotein is a functional homodimer requiring amino acids from both monomers in the catalytic centers [27]. FAD binds non-covalently and is thought to play a crucial role in ROS-generation [28]. Monomerization of LADH was proposed to occur due to mild acidification [8] or specific pathogenic mutations [27, 29], which could potentially account for the transformation of LADH to a diaphorase [8] and/or a Ser-protease [29], respectively. Later studies partly also by our laboratory, disproved monomer formation under the above conditions and proposed that instead, specific conformational changes would be responsible for the observed phenomena [3, 11, 30]. There are two additional reports on the crystal structure of hLADH; in these studies the protein was complexed to the E3-binding protein of hPDHc [30, 31]. In one of the studies the final experimental pH was not clearly stated [31], while in the other the final pH can only be estimated to be ~5-6. These papers conclude an overall 0.65-1.2 Å RMS deviation (Cα) amongst known E3 structures (from various species) [31], while there is no considerable structural change seen at the estimated pH=5-6 (see above) [30], relative to the free hLADH form measured at pH=7.0 [27]. Hence, there is hitherto no structural information available on the diaphorase/ROS-generating conformation. Nevertheless, pH dependence of the diaphorase/ROS-generating activity of LADH [3, 8, 10, 11] strongly suggests the involvement of a key residue with a pK_a in the range of the pH optimum of the diaphorase/ROS-generating activity.

Pathogenic mutations of LADH lead to a human disease called E3-deficiency [32]. They affect primarily tissues having high O_2 demand, hence often cause severe cardiological and neurological symptoms; the connection of genotype to biochemical and clinical symptoms is not yet fully understood [32, 33]. Clinical complications generally appear at the neonatal age and often lead to premature death [32, 34-44]. Pathogenic mutations of LADH reside mostly either in the cofactor-binding sites, or in the disulfide active center or in the dimerization surface [27, 32]. Our laboratory recently reported that four disease-causing

mutations (P453L, G194C, D444V, E340K) significantly increased the ROS-generating capacity of LADH [11]; three other pathogenic mutations were able to lower ROS generation by LADH. Consistent with this, it has been found that mutations with augmented ROS generation contributed to a loss of respiratory function (yeast model) due to oxidative damage occurring at the lipoic acid cofactor of PDHc and α-KGDHc [45]. These results show that elevated ROS generation by pathogenic mutants of LADH might directly contribute to the clinical presentations of E3-deficiency.

In the present work we examined the effects of nine pathogenic mutations and that of the pH on the structure of LADH by molecular dynamics simulation. We describe here the structural changes and identification of amino acids which may be involved in the development of the dysfunction and in the enhanced ROS-generating capacity of LADH.

Methods

Mutant structure building

For all the manipulations and calculations on the structures the programs VMD [46] and XPLOR-NIH [47] were used with standard applications of Linux. As for calculation architecture we used a 64-bit supercomputer running under a Solaris 9 operating system with 72 processors; no parallelization was applied. XPLOR-NIH was compiled in-house from source code and proper functionality was tested with the built-in XPLOR-NIH testing devices. We used the standard topology and parameter files supplied with XPLOR-NIH for proteins [48] (PROCHECK compatible), nucleic acids (for the AMP moiety of FAD), FMN, ions (K^+ and Cl^-) and H_2O with minor in-house modifications; the topology file for FAD was also generated in-house (for atom labeling, see Figure S1).

There are eight monomers in the asymmetric unit of crystals in the *1zmc* structure (A-H). We chose to work on monomers A and B that form a functional dimer. As a first step the structure and the pdb file of wt-LADH (*1zmc*) was manually modified to introduce the proper amino acid changes at the designated locations in the structure. In case of steric conflicts or close contacts the newly introduced side chain was further adjusted to achieve the best possible accommodation and a reasonable initial conformation. For some side chains, due to the manual processing of mutating the residues, stereochemistry needed to be corrected to the naturally occurring form (e.g. R(=L)-Cys for G194C; 2S,3R-Thr for I358T).

The pdb files also underwent further adjustments, as follows: the file format was fixed to be suitable for XPLOR-NIH, coordinates for H_2O, ions, NAD^+ were deleted (those of FAD were also temporarily deleted) and the two missing amino acids from the N-termini (E3-A) were modeled in: reasonable initial coordinates and then 500 steps of conjugate gradient energy minimization (from now on: energy minimization) was applied while atomic coordinates for residues 3-474 were kept fixed. For the B monomer (E3-B) the first three

amino acids were missing from the crystal structure and needed to be modeled in; to accommodate these residues minor shift of Pro4 was necessary, hence, during energy minimization residues 5-474 were fixed.

For nonbonded energy calculations the following settings and parameters were used: atom-by-atom cutoff for nonbonded list generation, constant dielectrics with shifting, dielectric constant (ε)=1.0, factor for 1-4 electrostatics (e_{14})=0.4, van der Waals switching, nonbonded interaction cutoff (r_{cut})=7.5 Å, effective switching distance (r_{on})=6.0 Å, switching/shifting function cutoff (r_{off})=6.5 Å; nonbonded interactions were excluded between bonded atoms and atoms bonded to a common third atom, but 1-4 interactions were computed (with 1-4 Lennard-Jones parameters and e_{14}) and explicit nonbonded exclusions in atom statements of amino acids were also taken into account. All default empirical (conformational and nonbonded) energy terms were applied with equal weights.

The *1zmc* structure contains only one disulfide bond (C45-C50) and two *cis* peptide bonds (H361-P362, H452-P453); the initial molecular structures were patched with these information. Before H-building, all non-H atoms were fixed and nonbonded energy terms were ignored; H-building was followed by energy minimization in 300 steps. Stereochemistry was verified after H-building throughout the structure. H-building was also applied for FAD. H-distances (to atoms of greater mass) were constrained by the SHAKE algorithm; SHAKE was applied during minimizations and MD runs for protein, FAD and H_2O molecules (where applied). For protein and FAD only bond lengths, while for H_2O, also bond angles were constrained in SHAKE; the number of maximum iterations were set to 100, the factor for tolerance was set to 0.01 (1 %), bond lengths and angles were referenced to the parameter file, in all cases.

To generate the initial structures for calculations simulating low pH (< 6.0), all twelve His residues were protonated at both nitrogen atoms; the twelve His constitute 2.5% of all

amino acids in LADH. After generating both monomers and the FADs, the dimer structures with the prosthetic groups in place were generated.

Gradual (stepwise) warming of structures

For MD simulations in H_2O, we applied the OPLS/TIP3P force field that modified the original TIP3P water model and made it suitable also to MD simulations [49, 50]; the application of this H_2O model demanded the usage of group-based cutoffs and the truncation function (for nonbonded interactions) during MD runs. A subset of coordinates for 125 H_2O molecules was retrieved from an XPLOR-NIH example file; after multiplication (to 64,000 H_2O molecules – 192,000 atoms (124 Å X 124 Å X 124 Å water box) *vs.* ~14,000 protein atoms(/dimer)) and trimming to a globular shape with a radius of 62 Å, it was applied for simulations (after ionization with 150 mM KCl in VMD). The actual ionized H_2O shell was created by uniting the E3 dimer (containing FAD) with the H_2O globe supplemented with ions, which was followed by deletion of H_2O and ions where they spatially conflicted (cutoff=2.6 Å) with protein or FAD. The protein dimer was eventually surrounded by a water shell with an average thickness of 12 Å.

For every structure in H_2O, first water with ions were energy minimized in 2,000 steps while E3 and FAD were fixed (friction coefficient (fbeta)=0 for all atoms, boundary potential (see below) and SHAKE constraints were in place; for all calculations in H_2O these last two conditions always applied). Afterwards, the whole system was energy minimized with no fixed atoms in another 2,000 steps and then a uniform initial distribution of velocities was assigned to all atoms. A gradual heating scheme for the structures were then initiated (10 K at a time) from 100 K (temperature used for recording X-ray diffraction pattern [27]) to 310 K (37 °C) permitting 10 ps simulation (equilibration) time at each temperature (10,000 steps with 1 fs integration time). The following parameters were used for treating nonbonded interactions during heat-up and all remaining MD runs (and their analysis): group-by-group

9

cutoff, constant dielectrics with truncation, r_{cut}=11.5 Å, nonbonded exclusions were treated as above and all the remaining parameters were of default. All default empirical energy terms and the one for boundary potential were applied with equal weights. The applied potential surface, to impede the escape of H_2O molecules during MD runs, was a deformable stochastic boundary potential developed by Brooks and Karplus [51, 52]; the boundary potential file was downloaded from the MMTSB website (http://mmtsb.org/webservices/sbmdpotential.html). The application of water molecules demanded the adjustment of the NMCATM parameter in the source/sbound.fcm file inside XPLOR-NIH; the program was recompiled from source code with the new parameter (NMCATM=100,000). To secure a soft gradual temperature equilibration scheme for the protein to 37 ^{o}C, the double-layered water shell approach delivered by Langevin dynamics (in Cartesian coordinate space), combined with the deformable stochastic boundary potential, was applied [51, 52]. Fbeta=62 was used for water oxygens in the Langevin buffer region (rbuf=52 Å) and fbeta=0 was applied to all atoms in the "reaction region" [52]; the Langevin boundary condition was monitored after each 5th step of MD.

MD runs at 37 ^{o}C

The resultant coordinates were set for further MD simulations at stable temperature (37 ^{o}C). In water, initiation of MD was preceded by 2,000 steps of energy minimization. The MD run consisted of 1.9 ns of simulation time (excluding the previous warm-up phase) with 1 fs time steps. As in this phase of MD, temperature control was switched from Langevin dynamics to temperature coupling (with a 310 K target temperature) [53], initial velocities were chosen to be reassigned using a Maxwellian initial distribution. The center-of-mass motion was removed with a frequency of 1,000 steps. MD simulations were all carried out in Cartesian coordinate space with the third-order Finite Difference Approximation approach

[52]. Coordinates were collected at every 500th step into binary coordinate trajectory files. Two parallel experiments were recorded in water by applying two different random seeds for the initial velocity assignments. Friction coefficients were set as follows: 62 for H_2O and 100 for all other atoms. All other conditions were the same as for the warm-up scheme.

MD without H_2O and ions

For MD runs without H_2O and ions, exactly the same procedures with the same parameters and settings, relevant to the protein and FAD, were applied as for the solvated protein except that parameters and settings relevant to H_2O and ions were left out from input files. Temperature control was set here by temperature-coupling throughout the warming-up phase and at 37 ^{o}C, as well. Simulation time was set to 9 ns excluding the warming-up period.

Analysis of trajectories

Trajectories recorded with or without water were analyzed and validated by the same procedures. First, RMS difference curves were calculated as a function of simulation time relative to the original initial structures. Trajectories were sampled in each recorded step and Cα coordinates of the E3 dimers were fit to the ones of the initial structures through translation and rotation (least-squares fitting [54]). After fitting, RMS differences were calculated for Cαs in the dimer and plotted against simulation time. RMSD curves were also created in parallel for each trajectory by fitting and calculating RMSDs for only those Cαs located in the actual domain that bears the respective pathogenic mutation and also for the ten amino acid stretch holding the mutation in its center position.

Samples of 10 ps length (it means 20 coordinate sets with 1 fs integration time and recording every 500th step to the trajectory file) were collected from the stable parts of the trajectories and were averaged. In some cases sampling needed to be repeated at a different

part of the trajectory, even for a very stable trajectory, to obtain well-behaving geometry for average structure.

Average structures were manually inspected and accepted if less than 10% of the peripheral part of the protein laid outside of the solvation sphere (by visual inspection). Average structures were energy minimized first in 2,000 steps with the following settings: all atoms but those of FAD were fixed, dihedral and improper energy terms were excluded and planarity restraints for the isoalloxazine ring, with a weight of 300 kcal mol^{-1} Å^{-2}, were implemented. In a second round of minimization in another 2,000 steps: the planarity energy term was excluded, the dihedral and the improper energy terms were included, and the isoalloxazine ring was fixed while all other atoms were loosened. During all minimizations proper SHAKE constraints were implemented. For structures simulated in water, after the last minimization step all water molecules and ions were deleted.

Validation of the final structures

Final structures were evaluated and validated by several means. All structures were analyzed for number of deviating bond lengths and angles inside XPLOR-NIH (thresholds: 0.1 Å for bonds and 10° for angles, relative to equilibrium values). Structures were accepted if they showed deviations only in the FAD cofactor (see Discussion) and they presented at least one of the two FADs with reasonably planar isoalloxazine ring, after manual inspection. Structures were further validated on the MOLPROBITY server (*molprobity.biochem.duke.edu*) for deviating bonds and angles, Cβ deviations (>0.25Å) and Ramachandran plots.

Fitting the structures

All final simulated mutant structures were fitted to the respective (in or without H_2O) final simulated wild-type "low pH" structure through the Cα atoms of the whole dimer; the respective RMSD values were also calculated. Comparisons of the structures after fitting were made in VMD and Pymol; some representative structure figures were created (see Figure 3, S4 and S5). Rendering structure figures was carried out with the internal ray-tracing facility of Pymol. Fittings and comparisons were also carried out to evaluate changes for all the simulated wild-type structures relative to the original *1zmc* structure and also between the wild-type structures with the protonated (low pH) and neutral (high pH) His residues. There have also been RMSD calculations between respective FAD residues (individual RMSDs) and also between final (protein) structures of the same mutations started with different seeds for velocity assignment during MD (in H_2O; to evaluate statistical significance of RMSD differences).

Residue displacement plots

Backbone and side-chain RMSDs were calculated on a *per* residue basis relative to the respective reference structures and were plotted against the residue numbers. Higher than 10 Å (for simulations in H_2O) or 7 Å (without H_2O) deviations were filtered and collected. Plots were calculated separately for the E3 A and B subunits (but plots for E3-B were not used for analysis, see Results).

Mapping specific inter-atomic distances (structure mapping)

Inter-atomic distances that represent specific interactions (FAD or NAD^+/NADH binding, monomer distance or LA-binding channel geometry) were identified in VMD and were measured inside XPLOR-NIH. Measurements were carried out only in the E3-A subunits (see Results). Comparison (and filtering) of distance values to ones from the

respective reference structures was performed in Excel. Among the 89 measured distances few also served as internal references: some distances (atom pairs) were used twice, in reverse order in syntax or applying the same residue pairs but with different atoms.

Results

Our first objective was to predict by molecular dynamics simulation the most relevant LADH conformation that is compatible with ROS generation. The other scope of this study was to reveal the structural changes in the ROS-generating LADH conformation caused by previously identified pathogenic mutations.

MD simulations in vacuum and in water plus ions

To achieve the first goal, protonation of the imidazole ring of all twelve His residues in LADH was carried out, since judging from the pK_a of the His side-chain (~6.0) most His residues at the pH optimum of the diaphorase/ROS-generating action (pH~5-6) are expected to be, at least partially, protonated. After carefully building up suitable mutant initial structures, we initiated nanosecond scale MD simulations on the structures in vacuum and in water *plus* ions. In the mutant structures all twelve His residues of LADH were also protonated; the wild-type structure was run with and without protonation, for controls. In all cases, in the first phase of the simulation the temperature was gradually increased from 100 K to 310 K (37 ^{o}C), then the development of the coordinate trajectory was recorded. In water, the warming phase of MD was driven by the gentler Langevin dynamics scheme applying a double layer water shell. To impede the escape of H_2O from the solvation sphere, a deformable stochastic boundary potential was applied. While Langevin dynamics worked satisfactorily during the relatively short warming up phase, it led to unstable temperature regulation on the ns scale, probably due to the great number of atoms in the system. Thus, temperature control was switched to the temperature-coupling scheme [53] with a constant target temperature of 37 ^{o}C for the ns scale simulations; this same temperature control scheme was used for simulations in vacuum, here also for the warming up phase. The potential surface around the outer boundary of the water shell (62 Å) was kept to impede the escape of

H$_2$O molecules; all water molecules were treated uniformly in this scheme. There was no H$_2$O escape through the boundary wall and temperature was stable throughout all MD experiments. This was also true for simulations in vacuum. Since simulations in water were launched with two different seeds for initial velocity assignments, two trajectories and two final structures were always generated.

Analysis of trajectory information

In most cases stabilizing trajectories could be recorded in terms of all the three RMSD curves followed, one for the full structure, one for the respective domain bearing the mutation and one for a 10 amino acid stretch having the pathogenic mutation in the center position. Since most trajectories in vacuum stabilized at around 2 ns, simulation time was set to the sum of ~2 ns in water to save computational capacity. For a few instances some more flexible loops or terminal stretches led to a continuously drifting (deviating) RMSD curve for the overall structure and then the stable part of the trajectory could only be judged by using the domain or sequence level difference curves (e.g. G194C in water [both structures] or M326V in water [structure #1]). In a few other cases, e.g. for K37E in water (structure #1) or R460G in water (structure #1), all three RMSD curves were continuously (or sometimes step-wise) and increasingly drifting; in these cases the most stable part of the trajectory was used for sampling. Interestingly, for E340K in vacuum or for L174F in water (structure #2), the 10 amino acid level curve drifted the most: for these cases it was concluded that the mutation led to a considerably less structured/stable or perturbed local environment with fewer/lost interactions for the newly introduced side chain, which did not manifest itself with the same magnitude in the overall structure. A representative RMSD curve set is displayed in Figure 1. Coordinate averaging was tried on stable trajectories, using up to a 500 ps averaging period, but such great time spans resulted in averaged structures with unsatisfactory geometry. 10 ps

averaging time, which equals to 20 consecutive coordinate sets, proved to be optimal for a good quality final structure. Final structures with less than 10% outlying peripheral amino acids from the water shell were energy minimized in two stages and validated. Only those structures were used, which showed bond length and bond angle deviations originating only from the FAD cofactor but not from the protein. Deviating bonds and angles in FAD structures may well arise from specific protein interactions and/or due to the insufficient experimental data in the applied FAD parameter files that determine the ideal equilibrium values. After inspection of each structure, only those were further analyzed that possessed at least one of the FAD cofactors in the structure with relatively planar isoalloxazine rings. Structures were further validated outside XPLOR-NIH on the independent MOLPROBITY server for deviating bonds and angles, Cβ deviations and Ramachandran plots. None of the finally approved structures possessed any deviating bonds, angles or Cβ deviations for the protein moiety. Ramachandran outliers were generally 3-4% for structures in water and 5-7% for structures in vacuum; outliers were almost always entirely borderline to the allowed regions as demonstrated with an example in Figure S2. Full H-building of the structures, protonation of the 12 His residues, interaction with FAD and for structures in water the interacting water and ions could all contribute to the Ramachandran plot analysis results.

Analysis of the wild-type structures

The wild-type structures simulated under different conditions can be seen in Figure 2 and Figure S3: the structure models were prepared with a higher (Figure 2) and a lower (Figure S3) sensitivity to secondary structure definition. It can be seen that MD simulation, as expected in the absence of explicitly imposed restraints, decreased the number of well-defined secondary elements under all simulation conditions, although the structure with protonated His residues ("low pH") in a solvated protein appear to have conserved them the most. It is

17

important to note that the "low pH" structures behaved better than the "high pH" ones and solvation helped the "low pH" structure better than the "high pH" one. These results further justify the application of both protonation of His and solvation and allow the suggestion that LADH might already contain one or more protonated His in structurally important position(s) at the pH of crystallization of *1zmc* (pH=7.0). It is also notable that the conformation of FAD was also altered in each case. The active center geometry was most preserved, with no specific restraints applied, in the "low pH" wild-type structure simulated in vacuum.

Analysis of the mutant structures

Final simulated mutant structures were fitted to the final simulated "low pH" wild-type structures for both simulation environments (Table 1). The final simulated "low pH" wild-type structures were fitted to the original *1zmc* structure (Figure 3) and also to the simulated "high pH" wild-type structures (Figure S4 and S5); the "high pH" wild-type structures were also compared to *1zmc* (see Table 1). Fitting was carried out using only the Cα atoms but from both monomers; RMSD calculations between structures were also based on this fitting algorithm that comprised translation and rotation. As a consequence, these overall RMSDs between structures also serve as measures for potential inter-monomeric displacements: from the magnitudes of the mutant RMSD values it can safely be concluded that none of the mutants displayed significant monomerization. The result is in accord with our previous data from size-exclusion chromatography and nano-LC ESI MS suggesting no monomerization upon mild acidification (down to pH=5.8) [3] or pathogenic mutations located even at the homodimerization surface of LADH [11]. For statistical evaluation of our fitting experiments, we also fitted and calculated RMSDs for structures of the same mutants, the simulations of which were commenced using different seeds for initial velocity assignment in water (Table S1). The average RMSD using all these structures was 6.92 Å and the respective S.E.M. was

18

0.59 Å. Hence, 6.92+0.59≅7.51 Å was set as a threshold value for RMSD difference for a mutant structure, relative to the "low pH" WT-LADH structure, to be designated as a significantly different structure. As seen in Table 1 all mutants (in water) reached this value. Such analysis was not performed for simulations in vacuum due to the absence of different initial seeds, and conclusions drawn in case of water simulations were considered applicable to structures in vacuum. Although, as a point of reference, another sample was taken from the trajectory of WT-LADH ("low pH") in vacuum. Fitting and RMSD calculation were performed relative to the originally sampled structure (last row in Table 1); the results suggest that structural changes in all the mutants can be considered significant in vacuum as well. Information in Table 1 show that the mutant structures, besides their significant deviations relative to the wild-type proteins, are compact and ordered. As expected, in a water *plus* ions environment structures deviate faster and generate greater RMSDs after the same lengths of simulation period. There are no great discrepancies in overall RMSDs amongst different simulated mutant structures, which is in concord with our former finding using circular dichroism (CD) spectroscopy where all the above mutants also exhibited barely distinguishable CD signatures [11]. These observations further strengthen the notion that the pathogenic mutant structures are still dimeric and well ordered and dysfunction evolves through specific conformational changes in the structure.

Residue displacement plots

To identify the amino acids, which most significantly change position at low pH and in the mutants, we calculated residue-level RMSD plots (residue displacement plots) relative to the *1zmc* structure or the simulated "low pH" wild-type structures. A representative plot can be seen in Figure 4. Due to the magnitudes of the RMSDs relative to the wild-type structures, mutant structure fittings are not shown individually; residue displacement results

and measurements from structure mapping (see below) were proved to be more informative in these cases. Residue displacement plots were created for all mutants (data not shown) comparing separately the E3-A and E3-B monomers, but results only from the E3-A monomers were used for interpretation since the isoalloxazine conformation was not completely satisfactory in E3-B monomers of the "low pH" wild-type simulated structures (neither in vacuum nor in water). We set a threshold limit of 10 or 7 Å in water *plus* ions or in vacuum, respectively, to filter amino acids that showed the highest degree of deviation relative to the reference structure; the higher limit to the solvated environment was applied since water and ions made the structures a little more extended. All structures were individually calculated and plotted and filtered amino acids were collected even if they could be filtered from only one of the structures. Displacements higher than 7 or 10 Å, respectively, were further filtered against a group of previously identified residues involved either in the active center, FAD-binding, NAD$^+$/NADH-binding, lipoic moiety-binding or homodimerization (see below and Table 2). In Table 2 asterisks label the residues, which dropped out more than once as a positive filtering result from the multiple analyses; more asterisks strengthen the likelihood that the particular residue is involved in the development of the respective alternative conformation of LADH.

Structure mapping

The original crystal structures *1zmc/1zmd* identified the residues that are in close contact or interaction with NAD$^+$/NADH or FAD. Also, the structure implies the presence and position of a binding channel for the lipoic acid moiety, although electron density could not be detected for exogenous LA used for soaking the crystals [27]. Amino acids could also be identified on the homodimerization surface of the dimer. It is known from previous mechanistic studies [15, 55-57] which residues take part in the catalytic action of LADH. On

this ground, we filtered further the residue displacement plots (see above), mapped the original crystal structure and identified individual atomic distances that represent these specific interactions and areas of the protein. We chose for instance, by manual selection, the most direct inter-atomic connections between the indicated residues (the functional group of the side chain, if applied) and FAD and measured the respective distances. For mapping the NAD^+/NADH binding site, as these molecules were omitted during simulation, the most direct distances were measured to FAD; FAD and NADH stack closely during catalysis, hence this approach proved to be applicable. To identify possible monomerization effects during simulation, three representative inter-domain distances were systematically screened. The putative LA-binding channel was thoroughly mapped, amino acids forming this channel were identified and representative inter-atomic distances were measured. All measured distances in mutants were compared to the respective ones in the appropriate (H_2O or no H_2O) wild-type "low pH" structures, and those that deviated with more than the factor of two are listed in Table 2 under "structure mapping". 89 specific distances were identified and measured for each mutant structure in vacuum and in water *plus* ions. Here again, only those structures were analyzed, which satisfied appropriate planarity measures for the isoalloxazine ring. In Table 2 amino acids are labeled by their functional locations; this way regions that are primarily affected by the mutations can be identified. To identify the structural changes, which are most likely associated with the transformation of LADH to a diaphorase/ROS-generator enzyme, the "low pH" wild-type structures were also compared to the *1zmc* structure (Table 2).

Data interpretation

As an example for data interpretation; for G194C it is seen from Table 2 that areas most affected by the mutation are the cofactor (FAD/NAD^+/NADH) binding sites; indeed we

previously measured ~30% decrease in FAD-binding for the isolated protein [11]. The crystallographic report [27] also suggested that cofactor-binding would be affected by G194C, but could not propose the involvement of any specific amino acids. Interestingly, we found that there is no considerable local perturbation in the structure of the G194C mutant around the position of the mutation (see Figure 4) contrary to the assumptions based on the crystallographic report on wt-hLADH [27]. The authors of that study could only make assumptions for the effects of the pathogenic mutations on the structure as they only had the wild-type structure in hand. Their proposition was that introduction of a rather polar and larger side-chain would make disturbance to the helix that bears G194 and this would have a negative effect on cofactor-binding; and again no exact amino acids could be ascribed to the changes, even on the local level. Our results suggest induction of structural perturbation at multiple sites in the protein, even farther in distance from the site of the mutation, which may help to explain the considerable loss of FAD-binding affinity due to G194C mutation.

Discussion

Mutations have different effects on protein structure: some mutations have negligible effects due to location or functional similarity while some other mutations have detrimental effects because they alter crucial interactions in the structure (pathogenic mutations). Mutations may have direct local effects but they can also trigger distant changes in the structure, even on the tertiary or the quaternary level. Mutations affecting ligand or cofactor binding may be critical, even if, generally multiple residues contribute to secure such interactions. In LADH, for instance, there are more than 35 residues in each monomer contributing to the strong (non-covalent) binding of FAD [27]. Yet, several (single) pathogenic mutations, some not even residing in the cofactor binding site, result in a considerably reduced affinity towards FAD [11, 55]. This study was initiated with the assumption that contrary to the suggestion by [27] local effects of mutations may not be sufficient to explain the pathogenecity of disease-causing mutations of hLADH, instead more complex alterations in the structure should be considered.

As detailed in the Introduction, LADH is greatly susceptible to the ambient conditions, and as many studies suggest, changes in LADH function are based on specific structural (conformational) changes [3, 8, 10, 11, 27, 29, 58]. It is important to note that several pathogenic mutations [30] or the drop in pH alone [3] can facilitate the dissociation of LADH from multienzyme complexes. These findings suggest that LADH might display some of its moonlighting functions as an independent enzyme (see also [25, 26]). Protein-protein interactions and conditions used for crystallography often shift conformational equilibria of proteins and stabilize the thermodynamically favored conformation under the existing conditions [59-63]. This conformation may considerably deviate from the uncomplexed or the solution structure [64-68]. Such effects may account for the lack of structural changes found in E3 when it was co-crystallized with the E3-binding protein of hPDHc at pH=~5-6. It is

possible that the delicate structural changes needed for the transformation to the diaphorase (ROS-generating) compatible conformation can only evolve in the uncomplexed form in solution. hPDHc binds E3 ~30 times stronger than KGDHc [26], which might be the reason why KGDHc is a stronger ROS producer than PDHc under pathological conditions. Since the structure of dimeric LADH (mass ~ 100 kDa) does not lend itself to solution NMR studies, we applied MD simulations to predict structural changes induced by pH (diaphorase conformation) and by known pathogenic mutations of the LADH protein. It was our intention to investigate the structural changes after heating the system up to 37 ^{o}C and also to see the effects of a physiologically relevant ionic strength in water.

Since the *1zmc* crystal structure is composed of 35% helices (18 helices) and 26% β-sheets (31 strands), the structure can be considered to be very compact. In such structures with stable secondary elements, little or no internal flexibility can be expected on the ps and ns (sometimes even on the ms) timescale [69], except maybe for some more mobile solvent-exposed loops. On the other hand, vibrations (of relatively freely moving and lighter atoms) and local rotations of molecular groups (if not hindered) are on the ps timescale [70]. Taking all these into consideration a ~10 ns simulation time was applied to record a stable trajectory in a molecular dynamics (MD) experiment to detect the effects of pH and pathogenic mutations on the LADH structure.

As there is no experimental data available yet on the diaphorase conformation of LADH, which could be used as structural restraints in the MD simulations, the accuracy of the presented structures cannot compete with a high-resolution crystal or NMR structure (although we applied the same force fields and simulation approaches which are routinely used in NMR and X-ray structure determination [47, 63, 65, 67, 68]). Nevertheless, we propose that the presented ("low pH") structures are closer to the real diaphorase solution structure, or the mutants of that, under ambient conditions than the crystal structures

determined so far for wt-hLADH. Being aware of the limits in the accuracy of our simulated structures, we propose to use these structures as the basis for further mechanistic studies aiming at the diaphorase/ROS-generating conformation and its mutated structures. Furthermore, even a well-determined crystal or solution structure demands further studies (e.g. kinetics, mutagenesis, etc.) to elucidate the mechanism of action. For the above purposes, we identified the most deviating amino acids, in terms of atomic positions, in functionally important regions of the LADH molecule (cofactor-binding sites, active center, LA-binding channel, monomerization surface) upon transformation to a diaphorase and after mutation (residue displacement plots). Additionally, approaching the analysis of structural changes from another aspect, we also described the most deviating structurally important distances in the above crucial regions (structure mapping). This information describes the predominant changes necessary for the structural switch from the native to the diaphorase/ROS-generating conformation and the ones that occur upon mutations. These are the primary information that this study offers. Obviously, amino acids and distances identified with deviations under the filter thresholds may also possess important structural information and may also induce functionally relevant changes to the structure, but our main objective in these simulations was to find the residues that were primarily affected. Residues (labeled with asterisks in Table 2) that dropped out for multiple occasions in different simulation experiments for the same molecules could be especially interesting. Analysis and validation of these changes may lead to new structural restraints/constraints that can be used to further refine these simulated structures until relevant high resolution NMR or X-ray structures become available.

Since we could not impose any structural restraints or constraints during MD all structural changes were allowed to develop with the maximum degrees of freedom. Since the water and ion models are less elaborated compared to the protein parameter files, simulation

results in water *plus* ions ought to be interpreted with more care. In fact, it is seen that the structures, although still compact and structured, are somewhat more "shaken apart" relative to the final structures in vacuum. This effect was also evident for the non-covalent dimerization interactions: when the "low pH" WT-LADH structure generated in water was compared to *1zmc*, a 9.91 Å RMSD was found when fitting was done for Cαs in both monomers, while this number was only 4.69 Å when we used only one of the monomers (and Cαs) for fitting. Nevertheless, the interactions with which water molecules and ions contributed to MD may be important towards the development of more realistic structural alterations. However, we handle the solvated structures as sources of information for detecting the short and long-range effects of mutations rather than real models of the mutant structures.

It is important to note that the *1zmc* structure was determined at pH=7.0, which is slightly more acidic than the physiological pH (~7.35 in the mitochondrial matrix). As crystal structures cannot detect hydrogens, it is not known which His residues, if any, are (or would be at pH=7.35) protonated in the wt-LADH structure (due to local effects leading to a perturbed pK_a); His is the foremost, but not the only, amino acid that is sensitive to protonation even at a pH farther away from its regular side-chain pK_a value. However, our result showing much less deviation from the crystal structure in active center geometry when all 12 His in the structure were protonated during MD suggests that wt-LADH likely has at least one structurally important His protonated at pH=7.0 or even 7.35; the active center ought to stay relatively intact even after heating to 37 ^{o}C or switching to the diaphorase conformation. Indeed, we found a His (H105) in the original *1zmc* crystal structure, which had two sets of coordinates; these two conformations might indeed represent a protonation equilibrium that is present already at pH=7.0 and is also manifested in structural changes. Without having an NMR structure of the protein or mutating systematically all His residues

but one and titrating the protein, there is no way of pin-pointing the protonation of crucial His residues. Nevertheless, H105 should be a target of further investigations. Protonating all His residues rather than using the original crystal structure with all non-protonated His residues (with H on only one of the imidazole nitrogens) is a reasonable trial to represent the diaphorase/ROS-generating conformation taking into account that the pH optimum of these activities (4.8-5.7) is lower than the side-chain pK_a of His (~6.0). Protonation of His residues in structurally significant positions, generally with a perturbed pK_a, often permits the formation of specific salt- or H-bridges that secure alternate conformations (the best example is hemoglobin).

Conclusions

Without the suggestion that any of our simulated LADH structures could precisely represent the actual structures on an atomic level precision, the amino acids identified here as being affected by the pH-drop and then by the pathogenic mutations can serve as good starting points for further mechanistic studies aiming to clarify the pathomechanisms related to the dysfunctions, mutations and ROS generation of LADH. Amino acids affected by the mutations in the diaphorase conformation may also contribute to the dysfunction of the physiological conformation.

A perspective approach to restore E3 activity in mitochondria might be enzyme replacement for which there are promising preliminary data [71]. Alternatively, rationally designed inhibitors against mutants with higher ROS generation and/or antioxidant therapy may be a future clinical perspective, for which deep insight into the structures is essential.

Acknowledgements

Conflict of Interest Statement. The authors declare no conflict of interest.

Figure Legends

Figure 1. Representative RMSD curves for the MD simulation trajectories of the P453L mutant of LADH ("low pH"). RMSDs were calculated for Cαs from both monomers relative to the initial structure in vacuum (**A**) or in water *plus* 150 mM KCl (structure #2) (**B**). The three curves with different colors represent (for A and B) RMSDs calculated using the full structure (blue), the domain carrying the actual mutation (pink) or a 10 amino acid stretch that holds the mutation in the center (green). Arrows designate the points of sampling the trajectories.

Figure 2. Structural models for *1zmc* and simulation results for wild-type LADH under different conditions. Conditions are designated above the respective models. Only monomer A is shown with different colors for domains: FAD-binding domain (1-149) - green, NAD$^+$/NADH-binding domain (150-282) - purple, central domain (283-350) - blue and interface domain (351-474) - orange. Structures were created and rendered in Pymol. A replica of this figure with a different sensitivity to secondary structure definition can be seen in Figure S3. A representative fitting result can be seen in Figure 3.

Figure 3. Fitting *1zmc* (blue) and the "low pH" WT-LADH structure after MD simulation in vacuum (orange). The four domains are separately presented for clarity reasons.

Figure 4. Representative residue displacement plot for the simulated G194C structure (#2) in water *plus* ions relative to the respective "low pH" wild-type structure. The plot represents RMS differences as a function of residue number after fitting the respective E3-A monomers. RMSDs are rms-averaged over the backbone atoms of each residue.

Figure 5. A representative plot of ratios of specific atomic distances for the P453L mutant relative to the respective wild-type "low pH" LADH structure in water *plus* ions. The serial numbers on the abscissa axis refer to the numbering scheme of distances in Figure S6. Ratios greater than 2 are filtered out from plots and collected in Table 2 under the "structure mapping" columns.

Figure S1. FAD structure and atom labeling applied in this study. This atom labeling scheme is referred to Figure S6 where specific atomic distances are designated for mapping the structure to describe principal intramolecular interactions.

Figure S2. Ramachandran plot of the simulated final structure of the G194C mutant of LADH in water *plus* 150 mM KCl (structure #2). 3.6% outliers were detected, but seemingly they are almost entirely borderline to the allowed regions.

Figure S3. This is a replica of Figure 2 with lower sensitivity to secondary structure definition. Structural models for *1zmc* and simulation results for wild-type LADH under different conditions are shown. Conditions are designated above the respective models. Only monomer A is shown with different colors for domains: FAD-binding domain (1-149) - green, NAD$^+$/NADH-binding domain (150-282) - purple, central domain (283-350) - blue and interface domain (351-474) - orange. Structures were created in VMD.

Figure S4. Structure fitting of the final simulation results in vacuum for "high pH" (blue) and "low pH" (red) wild-type structures. The four domains are separately presented for clarity reasons.

Figure S5. Structure fitting of the final simulation results in water *plus* ions for "high pH" (blue) and "low pH" (red) wild-type structures. The four domains are separately presented for clarity reasons.

Figure S6. Specific atomic distance definitions for structure mapping. Groups of selected atom-based distances represent specific interactions in the LADH molecule and were grouped in this figure accordingly; the type of interaction each group represents is in the header above each group in parenthesis. Selected distances were also used as internal references for the distance calculations (see text). All atomic distances were defined after manually inspecting the *1zmc* structure in VMD and taking also into account the structural information available on LADH in the PDB database.

References

[1]   A. Ambrus, B. Torocsik, V. Adam-Vizi, Protein Expr. Purif. 63 (2009) 50-57.

[2]   A. Ambrus, B. Torocsik, V. Adam-Vizi, Biochem. Eng. J. 45 (2009) 120-125.

[3]   A. Ambrus, L. Tretter, V. Adam-Vizi, J. Neurochem. 109 (2009) 222-229.

[4]   V. Massey, S. Strickland, S.G. Mayhew, L.G. Howell, P.C. Engel, R.G. Matthews, M. Schuman, P.A. Sullivan, Biochem. Biophys. Res. Commun. 36 (1969) 891-897.

[5]   F.M. Huennekens, R.E. Basford, B.W. Gabrio, J. Biol. Chem. 213 (1955) 951-967.

[6]   Y. Bando, K. Aki, J. Biochem. 109 (1991) 450-454.

[7]   C. Veeger, V. Massey, Biochim. Biophys. Acta 37 (1960) 181-183.

[8]   N.L. Klyachko, V.A. Shchedrina, A.V. Efimov, S.V. Kazakov, I.G. Gazaryan, B.S. Kristal, A.M. Brown, J. Biol. Chem. 280 (2005) 16106-16114.

[9]   V. Massey, Q.H. Gibson, C. Veeger, Biochem. J. 77 (1960) 341-351.

[10]   V. Massey, Biochim. Biophys. Acta 37 (1960) 314-322.

[11]   A. Ambrus, B. Torocsik, L. Tretter, O. Ozohanics, V. Adam-Vizi, Hum. Mol. Genet. 20 (2011) 2984–2995.

[12]   S. Ide, T. Hayakawa, K. Okabe, M. Koike, J. Biol. Chem. 242 (1967) 54-&.

[13]   L. Tretter, V. Adam-Vizi, J. Neurosci. 24 (2004) 7771-7778.

[14]   A.A. Starkov, G. Fiskum, C. Chinopoulos, B.J. Lorenzo, S.E. Browne, M.S. Patel, M.F. Beal, J. Neurosci. 24 (2004) 7779-7788.

[15]   F. Qi, R.K. Pradhan, R.K. Dash, D.A. Beard, BMC Biochem. 12 (2011) 53.

[16]   G. Zundorf, S. Kahlert, V.I. Bunik, G. Reiser, Neuroscience 158 (2009) 610-616.

[17]   E.B. Tahara, M.H. Barros, G.A. Oliveira, L.E.S. Netto, A.J. Kowaltowski, Faseb J. 21 (2007) 274-283.

[18]   V. Adam-Vizi, L. Tretter, Neurochem. Int. 62 (2013) 757-763.

[19]   M.J. Kumar, D.G. Nicholls, J.K. Andersen, J. Biol. Chem. 278 (2003) 46432-46439.

[20]   A.C. Nulton-Persson, L.I. Szweda, J. Biol. Chem. 276 (2001) 23357-23361.

[21]   L. Tretter, V. Adam-Vizi, J. Neurosci. 20 (2000) 8972-8979.

[22]   L.J. Yan, N. Sumien, N. Thangthaeng, M.J. Forster, Free Radical Res. 47 (2013) 123-133.

[23]   V.I. Bunik, C. Sievers, Eur. J. Biochem. 269 (2002) 5004-5015.

[24]   G.E. Gibson, A. Starkov, J.P. Blass, R.R. Ratan, M.F. Beal, Biochim. Biophys. Acta-Mol. Basis Dis. 1802 (2010) 122-134.

[25]   A. Constantinescu, U. Pick, G.J. Handelman, N. Haramaki, D. Han, M. Podda, H.J. Tritschler, L. Packer, Biochem. Pharmacol. 50 (1995) 253-261.

[26]   L.J. Reed, R.M. Oliver, Brookhaven Symp. Biol. 21 (1968) 397-412.

[27]   C.A. Brautigam, J.L. Chuang, D.R. Tomchick, M. Machius, D.T. Chuang, J. Mol. Biol. 350 (2005) 543-552.

[28]   A.I. Andreyev, Y.E. Kushnareva, A.A. Starkov, Biochemistry-Moscow 70 (2005) 200-214.

[29]   N.E. Babady, Y.P. Pang, O. Elpeleg, G. Isaya, Proc. Natl. Acad. Sci. USA 104 (2007) 6158-6163.

[30]   C.A. Brautigam, R.M. Wynn, J.L. Chuang, M. Machius, D.R. Tomchick, D.T. Chuang, Structure 14 (2006) 611-621.

[31]   E.M. Ciszak, A. Makal, Y.S. Hong, A.K. Vettaikkorumakankauv, L.G. Korotchkina, M.S. Patel, J. Biol. Chem. 281 (2006) 648-655.

[32]   J.M. Cameron, V. Levandovskiy, N. MacKay, J. Raiman, D.L. Renaud, J.T.R. Clarke, A. Feigenbaum, O. Elpeleg, B.H. Robinson, Am. J. Med. Genet. A 140A (2006) 1542-1552.

[33]   A. Saada, I. Aptowitzer, G. Link, O.N. Elpeleg, Biochem. Biophys. Res. Commun. 269 (2000) 382-386.

[34]   Y.S. Hong, S.H. Korman, J. Lee, P. Ghoshal, Q. Qu, V. Barash, S. Kang, S. Oh, M. Kwon, A. Gutman, A. Rachmel, M.S. Patel, J. Inherit. Metab. Dis. 26 (2003) 816-818.

[35]   O. Grafakou, K. Oexle, L. van den Heuvel, R. Smeets, F. Trijbels, H.H. Goebel, N. Bosshard, A. Superti-Furga, B. Steinmann, J. Smeitink, Eur. J. Pediatr. 162 (2003) 714-718.

[36]   E. Shany, A. Saada, D. Landau, A. Shaag, E. Hershkovitz, O.N. Elpeleg, Biochem. Biophys. Res. Commun. 262 (1999) 163-166.

[37]   A. Shaag, A. Saada, I. Berger, H. Mandel, A. Joseph, A. Feigenbaum, O.N. Elpeleg, Am. J. Med. Genet. 82 (1999) 177-182.

[38]   Y.S. Hong, D.S. Kerr, T.C. Liu, M. Lusk, B.R. Powell, M.S. Patel, Biochim. Biophys. Acta-Mol. Basis Dis. 1362 (1997) 160-168.

[39]   Y.S. Hong, D.S. Kerr, W.J. Craigen, J. Tan, Y.Z. Pan, M. Lusk, M.S. Patel, Hum. Mol. Genet. 5 (1996) 1925-1930.

[40]   T.C. Liu, H. Kim, C. Arizmendi, A. Kitano, M.S. Patel, Proc. Natl. Acad. Sci. USA 90 (1993) 5186-5190.

[41]   S.C. Quinonez, S.M. Leber, D.M. Martin, J.G. Thoene, J.K. Bedoyan, Pediatr. Neurol. 48 (2013) 67-72.

[42]   A. Font, E. Quintana, M.A. Vilaseca, F. Tort, A. Ribes, M. Pineda, P. Briones, J. Inherit. Metab. Dis. 33 (2010) S79-S79.

[43]   M.H. Odievre, D. Chretien, A. Munnich, B.H. Robinson, R. Dumoulin, S. Masmoudi, N. Kadhom, A. Rötig, P. Rustin, J.P. Bonnefont, Hum. Mutat. 25 (2005) 323-324.

[44]   O.N. Elpeleg, A.B. Saada, A. Shaag, J.Z. Glustein, W. Ruitenbeek, I. Tein, J. Halevy, Muscle Nerve 20 (1997) 238-240.

[45]   R.A. Vaubel, P. Rustin, G. Isaya, J. Biol. Chem. 286 (2011) 40232-40245.

[46]   W. Humphrey, A. Dalke, K. Schulten, J. Mol. Graph. Model. 14 (1996) 33-38.

[47]   C.D. Schwieters, J.J. Kuszewski, G.M. Clore, Prog Nucl Mag Res Sp 48 (2006) 47-62.

[48]   R.A. Engh, R. Huber, Acta Crystallogr. A. 47 (1991) 392-400.

[49]   W.L. Jorgensen, J. Chandrasekhar, J.D. Madura, R.W. Impey, M.L. Klein, J. Chem. Phys. 79 (1983) 926-935.

[50]   L.X. Dang, B.M. Pettitt, J. Phys. Chem. 91 (1987) 3349-3354.

[51]   C.L. Brooks, M. Karplus, J. Chem. Phys. 79 (1983) 6312-6325.

[52]   A. Brunger, C.L. Brooks, M. Karplus, Chem. Phys. Lett. 105 (1984) 495-500.

[53]   H.J.C. Berendsen, J.P.M. Postma, W.F. Vangunsteren, A. Dinola, J.R. Haak, J. Chem. Phys. 81 (1984) 3684-3690.

[54]   W. Kabsch, Acta Crystallogr. A. 32 (1976) 922-923.

[55]   T.C. Liu, L.G. Korotchkina, S.L. Hyatt, N.N. Vettakkorumakankav, M.S. Patel, J. Biol. Chem. 270 (1995) 15545-15550.

[56]   H. Kim, M.S. Patel, J. Biol. Chem. 267 (1992) 5128-5132.

[57]   I.G. Gazaryan, B.F. Krasnikov, G.A. Ashby, R.N.F. Thorneley, B.S. Kristal, A.M. Brown, J. Biol. Chem. 277 (2002) 10064-10072.

[58]   J. Visser, C. Veeger, Biochim. Biophys. Acta 159 (1968) 265-275.

[59]   A. Ambrus, I. Banyai, M.S. Weiss, R. Hilgenfeld, Z. Keresztessy, L. Muszbek, L. Fesus, J. Biomol. Struct. Dyn. 19 (2001) 59-74.

[60]   A. Ambrus, K. Friedrich, A. Somogyi, Anal. Biochem. 352 (2006) 286-295.

[61]   A. Ambrus, D. Yang, Anal. Biochem. 367 (2007) 56-67.

[62]   M. Palczewska, P. Groves, A. Ambrus, A. Kaleta, K.E. Kover, G. Batta, J. Kuznicki, Eur. J. Biochem. 268 (2001) 6229-6237.

[63]   S.A. Roberts, G.F. Wildner, G. Grass, A. Weichsel, A. Ambrus, C. Rensing, W.R. Montfort, J. Biol. Chem. 278 (2003) 31958-31963.

[64]   A. Ambrus, D. Chen, J.X. Dai, T. Bialis, R.A. Jones, D.Z. Yang, Nucleic Acids Res. 34 (2006) 2723-2735.

[65]   A. Ambrus, D. Chen, J.X. Dai, R.A. Jones, D.Z. Yang, Biochemistry 44 (2005) 2048-2058.

[66]   J.X. Dai, A. Ambrus, L.H. Hurley, D.Z. Yang, J. Am. Chem. Soc. 131 (2009) 6102-6104.

[67]   J.X. Dai, T.S. Dexheimer, D. Chen, M. Carver, A. Ambrus, R.A. Jones, D.Z. Yang, J. Am. Chem. Soc. 128 (2006) 1096-1098.

[68]   J.X. Dai, C. Punchihewa, A. Ambrus, D. Chen, R.A. Jones, D.Z. Yang, Nucleic Acids Res. 35 (2007) 2440-2450.

[69]   S. Grzesiek, A. Bax, J.S. Hu, J. Kaufman, I. Palmer, S.J. Stahl, N. Tjandra, P.T. Wingfield, Protein Sci. 6 (1997) 1248-1263.

[70]   M.H. Levitt, Spin dynamics: Basics of nuclear magnetic resonance, John Wiley and Sons West Sussex, England, 2006.

[71]   M. Rapoport, A. Saada, O. Elpeleg, H. Lorberboum-Galski, Mol. Ther. 16 (2008) 691-697.

Figure 1

A

no H$_2$O or ions

full structure

RMSD (Å)

domain

10 amino acid stretch

simulation time (ns)

B

H$_2$O and ions

RMSD (Å)

simulation time (ps)
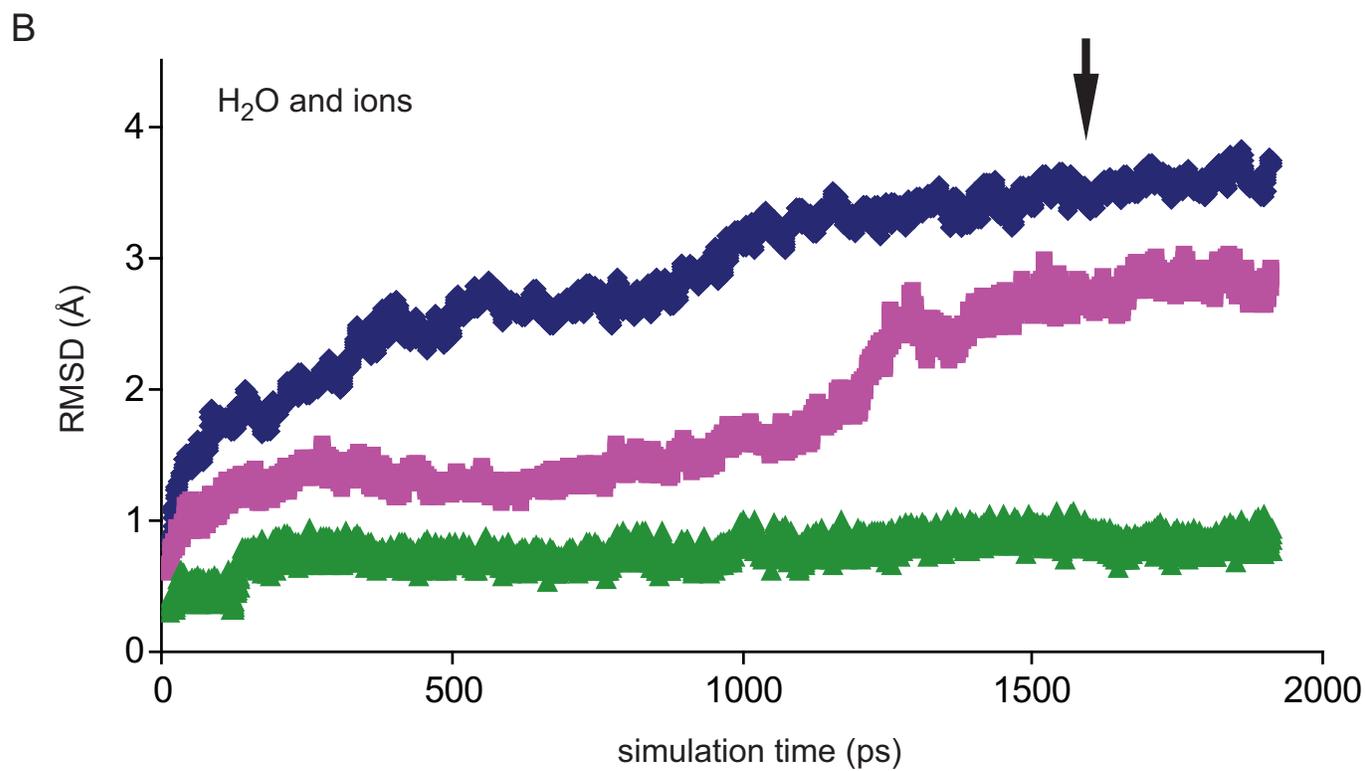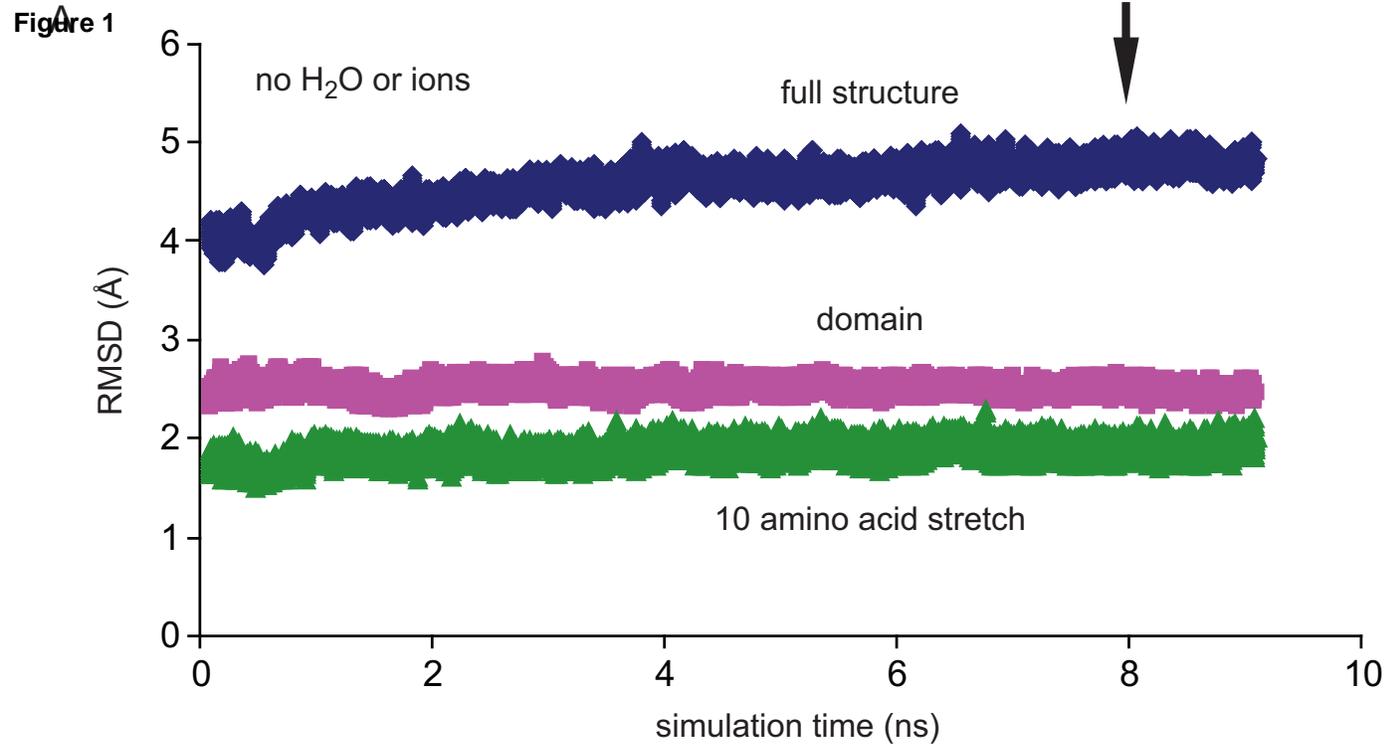
Figure 1.

Figure 2 *1zmc* **WT-LADH, "high pH", no H₂O/ions**
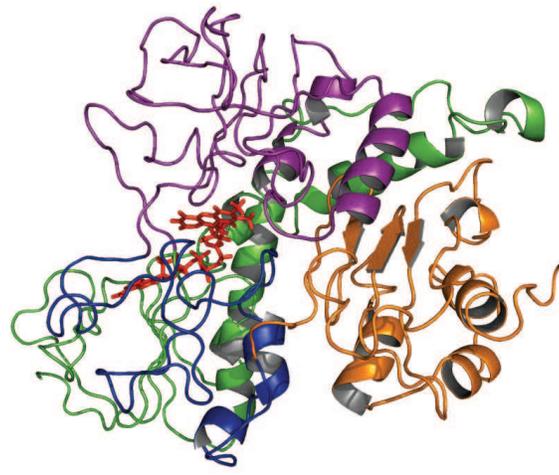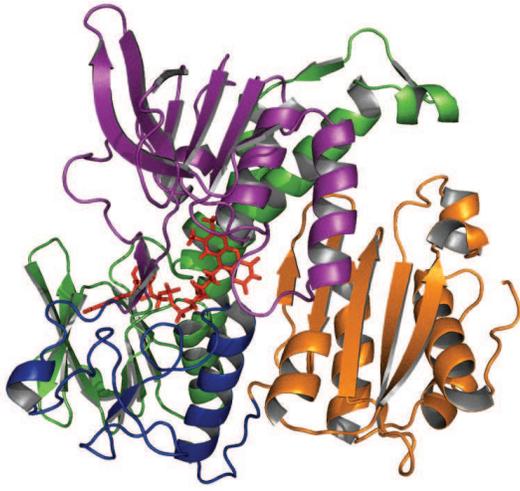
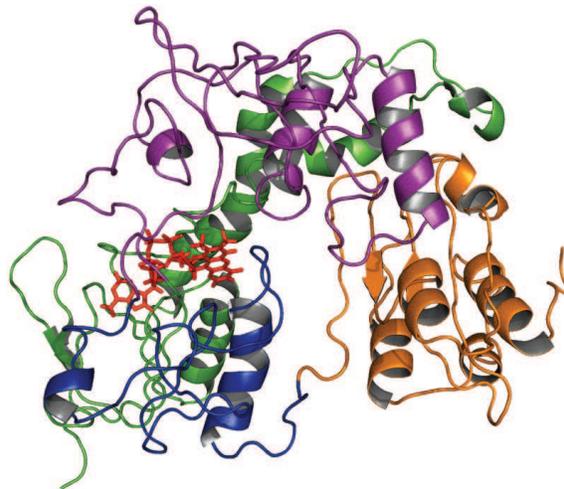**WT-LADH, "high pH", H₂O/ions** **WT-LADH, "low pH", no H₂O/ions**
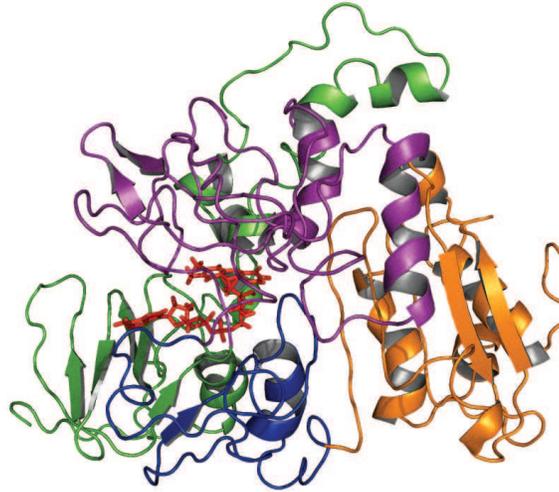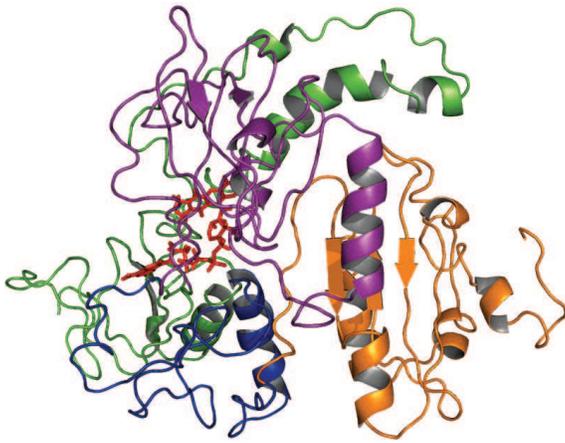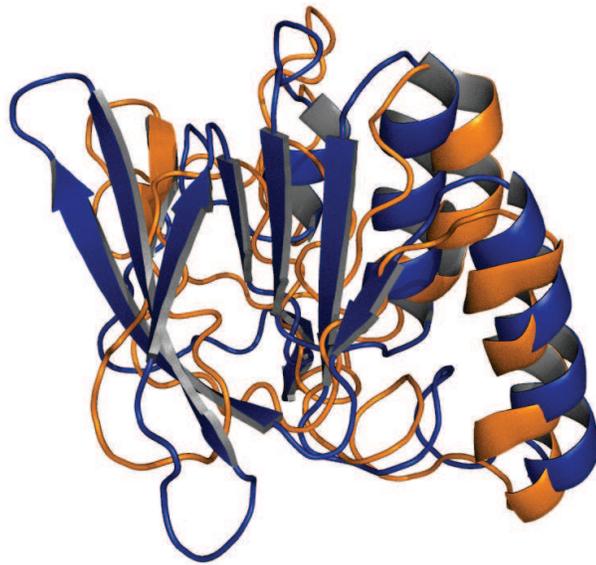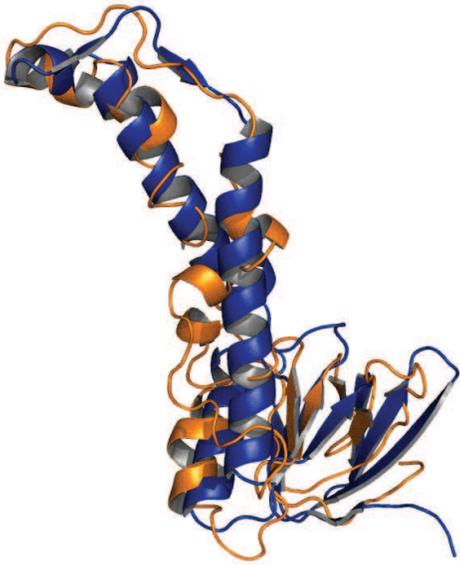
WT-LADH, "low pH", H₂O/ions

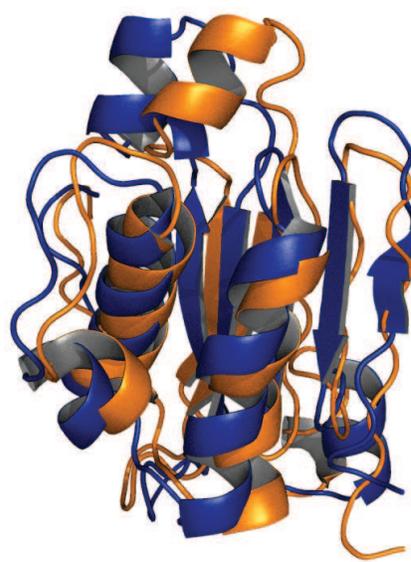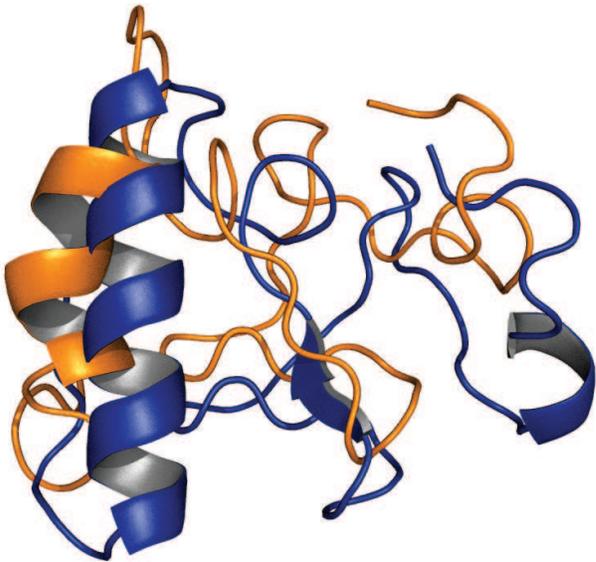Figure 2.

Figure 3
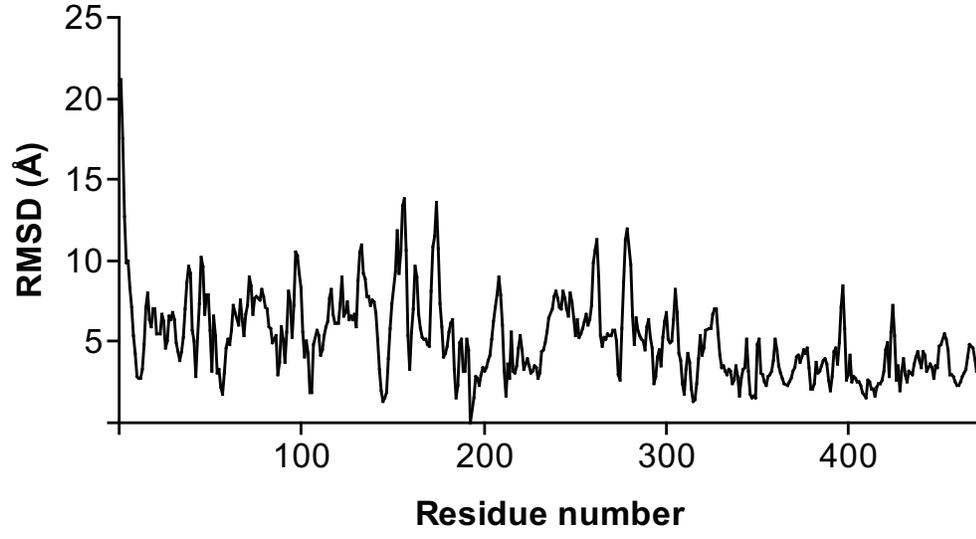
domain 1

domain 2

domain 3

domain 4

Figure 3.

Figure 4

Figure 4.

Figure 5

serial number for specific distance
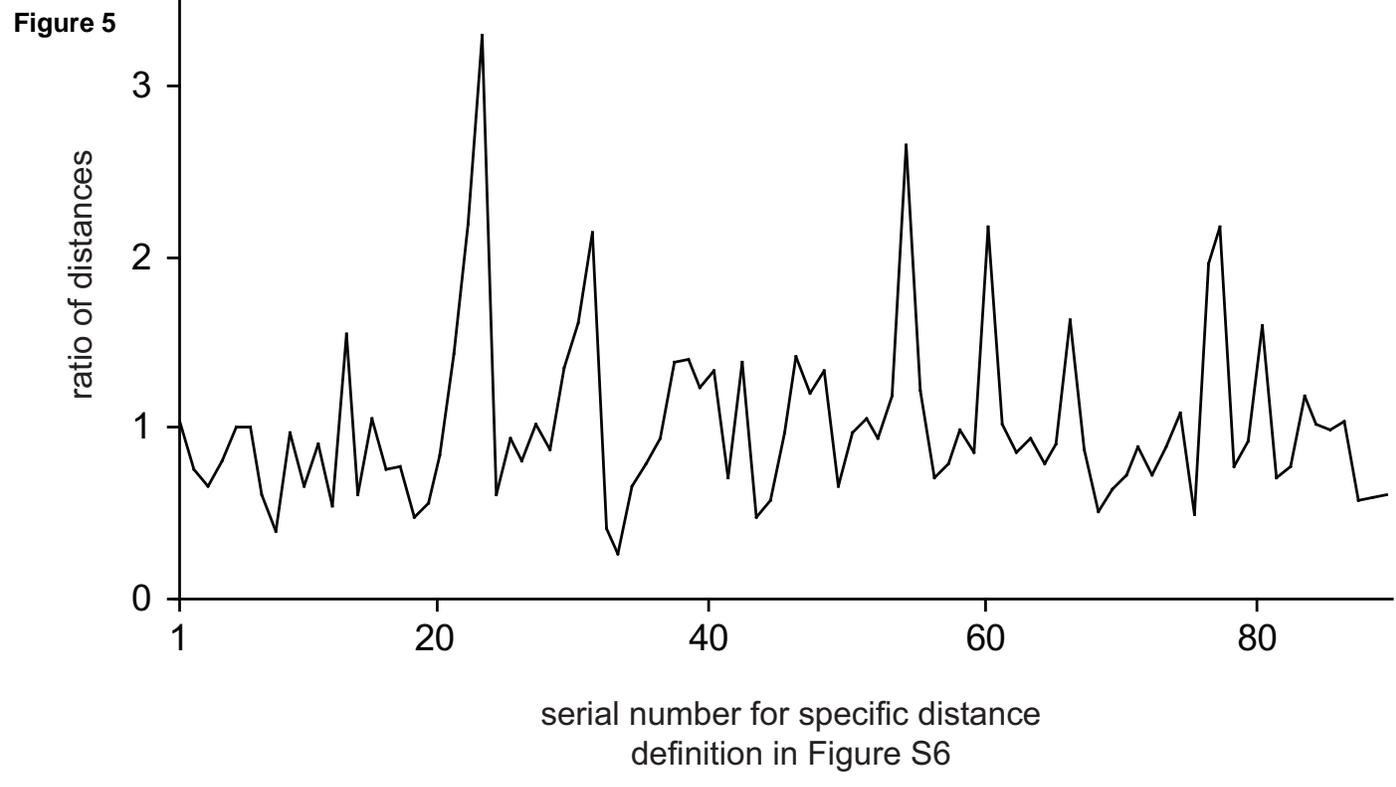definition in Figure S6

Figure 5.

Table 1

Table 1. Fitting simulated structures to reference structures.[a]

Structure	Reference	RMSD (Å, protein)	RMSD (Å, FAD-A)	RMSD (Å, FAD-B)
WT-LADH #1	*1zmc*	7.78	2.81	4.29
WT-LADH #1-lowpH	*1zmc*	9.91	3.94	5.75*
WT-LADH #1-lowpH	WT-LADH #1	9.58[d]	4.44	4.43
D444V #2	WT-LADH #1-lowpH	10.62	4.12	4.72
K37E #1	WT-LADH #1-lowpH	9.72	3.26	4.29
K37E #2	WT-LADH #1-lowpH	9.23	3.84*	5.27
G194C #1	WT-LADH #1-lowpH	10.92	3.96	5.49
G194C #2	WT-LADH #1-lowpH	9.55	4.88	5.10
P453L #2	WT-LADH #1-lowpH	10.11	3.82*	4.79
M326V #1	WT-LADH #1-lowpH	10.10	5.49	4.44
I358T #1	WT-LADH #1-lowpH	8.79	4.34	4.08
I358T #2	WT-LADH #1-lowpH	7.51	4.35	4.22
E340K #2	WT-LADH #1-lowpH	9.08	3.76	6.12
R460G #1	WT-LADH #1-lowpH	11.11	4.33	4.80
R460G #2	WT-LADH #1-lowpH	11.61	4.84	4.88
L174F #1	WT-LADH #1-lowpH	11.92	3.31	3.67*
WT-LADH	*1zmc*	4.51	4.07	3.02*
WT-LADH -lowpH	*1zmc*	4.58[b]	3.36	3.40*
WT-LADH -lowpH	WT-LADH #1	4.91[c]	5.05	3.16*
D444V	WT-LADH -lowpH	4.87	2.09	4.63
K37E	WT-LADH -lowpH	5.06	4.17	4.10
G194C	WT-LADH -lowpH	4.14	2.97	4.26
P453L	WT-LADH -lowpH	4.53	3.78	3.89
M326V	WT-LADH -lowpH	5.00	2.64	3.76
I358T	WT-LADH -lowpH	4.77	2.45*	3.10
E340K	WT-LADH -lowpH	5.33	3.34	3.66*
R460G	WT-LADH -lowpH	6.29	3.62	4.33
L174F	WT-LADH -lowpH	4.81	3.00	4.51*
WT-LADH –lowpH – 3.0 ns	WT-LADH –lowpH – 6.5 ns	1.49	1.87	1.91

[a] RMSDs are calculated for Cα atoms only, but from both monomers. Data above the bold separation line are from simulations in water *plus* ions while under the line are from simulations in vacuum. Structures having deviating bond lengths or angles in the protein moiety were not examined and included here and also were not used for further analysis. Asterisks label FADs that were not approved for planar isoalloxazine ring and were not used for further analysis; this label relates to the structure under investigation, not the reference. [b] For structure fitting, see Figure 3. [c] For structure fitting, see Figure S4. [d] For structure fitting, see Figure S5.

Table 2

Table 2. The most deviating amino acids identified according to residue displacement plots and structure mapping.[a]

Protein	Residue displacement (water *plus* ions)	Residue displacement (vacuum)	Structure mapping (water *plus* ions)	Structure mapping (vacuum)
G194C	46_l, 99_l, 155_n^{**}, 278_n, 279_n^*, 280_f^*	43_f, 44_f, 49_f, 155_n^{**}	277_n^*, 332_l-99_l^*, 99_l-51_l, 51_l-$453'_l^*$	45_l-328_l, 99_l-$392'_l$, 51_l-$453'_l^*$
P453L	155_n, 473_l	42_l, 46_l, 99_l, 43_f, 44_f, 48_f, 49_f, 150_f, 280_f, 45_a	118_f, 119_f, 283_f, 277_n, 51_l-$452'_l$	45_a-$452'_a$, 50_a-$452'_a$, 13_f, 36_f, 37_f,
E340K	155_n	-	332_l	13_f, 36_f, 37_f, 38_f, 320_f, 188_n, 192_n
I358T	155_n^*, 279_n^*, 280_f	149_f, 168_f, 279_n^*	277_n, 51_l-$453'_l$, 392_l-453_l	36_f, 37_f, 99_l-$392'_l$
K37E	46_l^*, 103_l, 99_l, 155_n^*, 279_n^*, 280_f^*, 438_d	42_l, 46_l^*, 43_f, 44_f, 48_f, 49_f, 117_f, 150_f, 168_f, 280_f^*, 326_f, 45_a, 279_n^*	444_d-$438'_d$, 277_n	45_a-$452'_a$, 50_a-$452'_a$, 12_f, 13_f, 35_f, 36_f, 37_f, 117_f, 119_f, 168_f, 320_f
M326V	99_l, 473_l, 168_f, 280_f^*, 209_n, 210_n	42_l, 43_f, 44_f, 48_f, 49_f, 117_f, 280_f^*, 279_n	36_f^*, 148_f, 168_f, 277_n, 51_l-$452'_l$, 332_l-99_l, 51_l-$453'_l$	45_a-$452'_a$, 12_f, 13_f, 36_f^*, 37_f, 119_f, 147_f, 99_l-$392'_l$
R460G	155_n^{**}, 280_f^*, 49_f	15_f, 16_f, 17_f, 43_f, 44_f, 117_f, 150_f, 168_f, 280_f^*, 320_f, 42_l, 46_l, 99_l, 103_l, 155_n^{**}, 279_n, 340_d	118_f, 168_f, 277_n^*, 45_l-328_l, 51_l-$452'_l$, 332_l-99_l^*, 99_l-51_l, 51_l-$453'_l^*$, 99_l-$392'_l^*$, 103_l-$452'_l$	50_a-FADn5r$_a$, 37_f, 444_d-$438'_d$, 188_n, 192_n, 99_l-$392'_l^*$
D444V	46_l, 155_n^*	49_f, 99_l, 155_n^*	392_l-453_l	12_f, 13_f, 35_f, 36_f, 37_f, 38_f, 117_f, 118_f, 119_f, 147_f
L174F	99_l^*, 473_l, 155_n, 279_n^*, 280_f^*, 283_f	37_f, 38_f, 43_f, 44_f, 117_f, 118_f, 280_f^*, 42_l, 99_l^*, 103_l, 279_n^*	283_f, 444_d-$438'_d$, 99_l-$392'_l^*$, 332_l-99_l, 99_l-51_l, 51_l-$453'_l^*$	12_f, 36_f, 37_f, 45_l-328_l, 99_l-$392'_l^*$, 51_l-$453'_l^*$
"low pH" LADH	155_n, $[156$-$158]^*$, 174, 175, 262, 263	28, 29, 38_f, 39, 42_l, 43_f, 100, 109, 123, 138, $[156$-$158]^*$, $[164$-169 $(168_f)]$, 171, 172, $[247$-$255]$, 265, 266, 270, 272, $[290$-$294]$, $[298$-$300]$, 344, 376, 396	45_a-$452'_a$, 15_f^*, 17_f^*, 49_f, 53_f, 54_f^*, 320_f, 326_f, 46_l-51_l^*, 46_l-99_l^*, 473_l-452_l, 332_l-19_l^*, 473_l-457_l	$[15^*$-$17^*]_f$, 43_f, 44_f, 45_f-16_f, 54_f^*, 148_f, 280_f, 283_f, $[326^*$-$329]_f$, 453_f, 51_l-$452'_l$, 452_l-392_l, 46_l-51_l^*, 46_l-99_l^*, 453_l-452_l, 19_l-$452'_l$, 332_l-19_l^*, 328_l-$452'_l$

[a] In residue displacement plots the greater deviations of stretches of the N- and C-terminii were neglected from the above selections. Amino acid numbering is based on 474 amino acids

(mature protein). Only those amino acids are designated here for residue displacement plots that went positively through a double filter: 1. more than 7 (vacuum) or 10 Å (water *plus* ions) displacement relative to the respective reference structure, and 2. previously identified as being a participant in a crucial interaction in the original *1zmc* structure (see text). For residues designated here as positive results from structure mapping needed to pass a filter of presenting with a more than 2 times factor for designated atom distance relative to the reference structure. Only for "low pH" LADH structure: for residue displacement plots all designated residues passed the first filter, and the second filter was not used (to detect changes in all areas of LADH) and a filter factor of 3 was used for structure mapping in water *plus* ions (see text). Asterisks designate residues positively filtered from multiple analyses (e.g. in vacuum and in water or in both of the structures in water); the number of asterisks designates how many times that residue was filtered positively out (double asterisks mean three positives, etc.). All structures were individually plotted and filtered amino acids are designated even if they are filtered from only one of the analyses (but fulfilled the requirements of the double filter). Subscript codes for amino acid locations: active center – a, FAD-binding site – f, NAD$^+$/NADH-binding site – n, lipoic moiety binding site – l, dimer interface – d; this way regions most affected by the mutation can be identified. Some residues belong to multiple categories. The ' sign after residues designate in structure mapping data (when residue pairs are given) that the residue belongs to the other monomer. Brackets mean ranges of amino acids.